RSC Advances

PAPER

View Article Online
View Journal | View Issue

Check for updates

Cite this: *RSC Adv.*, 2021, **11**, 6107

Boosting the hydrogen evolution reaction activity of Ru in alkaline and neutral media by accelerating water dissociation†

Lin Tang, Junjie Yu, Yang Zhang, Zaozao Tang and Yong Qin *

Electrochemical water splitting *via* a cathodic hydrogen evolution reaction (HER) is an advanced technology for clean H_2 generation. Ru nanoparticle is a promising candidate for the state-of-the-art Pt catalyst; however, they still lack the competitiveness of Pt in alkaline and neutral media. Herein, a ternary HER electrocatalyst involving nano Ru and Cr_2O_3 as well as N-doped graphene (NG) that can work in alkaline and neutral media is proposed. Cr_2O_3 and NG feature strong binding energies for hydroxyl and hydrogen, respectively, which can accelerate the dissociation of water, whereas Ru has weak hydrogen binding energy to stimulate hydrogen coupling. The HER activity of Ru is greatly enhanced by the promoted water-dissociation effect of NG and Cr_2O_3. To achieve a current density of 10 mA cm^{-2}, the as-obtained Ru–Cr_2O_3/NG only needs a very low overpotential of 47 mV, which outperforms the activity of Pt/C in alkaline media. The strategy proposed here, multi-site acceleration of water dissociation, provides new guidance on the design of a highly efficient, inexpensive, and biocompatible HER catalyst in nonacidic condition.

Received 9th November 2020
Accepted 19th January 2021

DOI: 10.1039/d0ra09515j

rsc.li/rsc-advances

Open Access Article. Published on 03 February 2021. Downloaded on 2/8/2026 6:22:50 PM.
This article is licensed under a Creative Commons Attribution-NonCommercial 3.0 Unported Licence.

1. Introduction

Renewable energy sources have drawn great attention due to the ever-growing global energy crisis and environmental deterioration. As a kind of clean energy, hydrogen is one of the most promising candidates to replace fossil fuels; unfortunately, this hype has so far been elusive because hydrogen production from water is quite difficult in nature.[1] Electrochemical water-splitting is a potential solution for the production of hydrogen with high purity.[2] Hydrogen evolution reaction (HER) is one of the two critical half-reactions in electrochemical water-splitting. To conduct HER smoothly, voltages above the thermodynamic potential (known as overpotential) must be applied. Reducing the overpotential is essential to make hydrogen production less energy-intensive, which can be achieved by an efficient electrocatalyst. Pt is hitherto the most active electrocatalyst toward HER; however, the rarity and high cost are big hurdles for practical commercialization.[3] Currently, the exploration of low-cost alternatives to Pt is a crucial technological task in developing a hydrogen economy. Although transition metal derivative (oxides,[4–6] sulfides,[7–9] phosphides,[10–13] carbides,[14–16] and nitrides[17–19]) catalysts have been widely pursued as candidates, they still lack the competitiveness of Pt; moreover, most of them can only function in acidic condition.

Actually, HER conducted in alkaline and neutral media is more advantageous than that in acidic media, for example, reduced environmental pollution and equipment corrosion. Especially, electrolyzers working in neutral conditions can potentially allow the direct utilization of salt water, the most abundant resource on earth, which can make electrochemical hydrogen production more inexpensive and eco-friendly. However, HER in alkaline and neutral media is still a formidable challenge because their kinetics is commonly decelerated by an extra water dissociation step. The state-of-the-art Pt catalyst in neutral media expresses two or three orders of magnitude lower activity than in acidic media.[20] At present, finding a competent HER catalyst in non-acidic media is very imperative to speed up the development of clean hydrogen production.

It has been discovered that water-splitting in neutral and alkaline media begins with a water-dissociation step and follows either the electrochemical Heyrovsky or the chemical Tafel recombination step.[21] Therefore, the overall activity of a catalyst in non-acidic media is not only determined by the capability to catalyze H^+ into H_2, but also by the kinetics of water dissociation on the interface. Previous studies to improve the kinetics of water dissociation were focused on the introduction of an additional catalyst with strong OH binding energy, such as metal oxides and metal hydroxides (M–OH),[22] or the surface texturing of the catalyst.[23] Very recently, Sargent *et al.* found a more effective strategy of using a multi-site electrocatalyst

Jiangsu Key Laboratory of Advanced Materials and Technology, School of Petrochemical Engineering, Changzhou University, Changzhou, Jiangsu, 213164, China. E-mail: qinyong@cczu.edu.cn

† Electronic supplementary information (ESI) available: Experimental section, the SEM image, the XPS survey, the ECSA, the TOF value, the EIS and the cycling stability of the catalysts. See DOI: 10.1039/d0ra09515j

© 2021 The Author(s). Published by the Royal Society of Chemistry

Open Access Article. Published on 03 February 2021. Downloaded on 2/8/2026 6:22:50 PM.
This article is licensed under a Creative Commons Attribution-NonCommercial 3.0 Unported Licence.

(CrO_x/Cu–Ni) containing two sites with strong binding energies for hydrogen (Ni site) and hydroxyl groups (CrO_x site),[24] respectively, to accelerate water dissociation. In combination with a third site (Cu site) that has a weak hydrogen binding energy to stimulate hydrogen coupling, the composite catalyst exhibited exceptional HER activity in a pH 7 buffer electrolyte.

Ru is a cheaper noble metal than Pt, and it exhibits a similar hydrogen bond energy to that of Pt (65 kcal mol^{-1});[25,26] thus, it is a promising alternative to Pt in HER. After the rational texturing design, Ru has exhibited intriguing HER performance in acidic media;[27] however, it's performance is still far from satisfactory in alkaline and neutral media. Herein, based on the principle of promoting the kinetics of water dissociation, we designed a ternary catalyst comprising Ru, Cr_2O_3, and N-doped graphene (NG), denoted as Ru–Cr_2O_3/NG, in which Cr_2O_3 strongly binds OH and NG strongly binds H, respectively, to jointly accelerate the dissociation of water; meanwhile, Ru has a weak hydrogen binding energy, to push hydrogen coupling. As expected, the HER activity of Ru in alkaline and neutral media is significantly enhanced by the synergistic effect with Cr_2O_3 and NG.

2. Experimental

2.1 Preparation of Ru–Cr_2O_3/NG

The preparation of NG can be found in our previous work.[28] Dissolve 30 mg tri(2,2′-bipyridine) ruthenium dichloride hexahydrate [$Ru(bpy)_3$], 3.2 mg $Cr(NO_3)_3 \cdot 9H_2O$, and 30 mg cyanuric acid in 2.0 mL *N*,*N*-dimethyl formaldehyde (DMF), and then disperse 20 mg NG into the above solution by ultrasound. The mixture was dried in air at room temperature. After annealing at 750 °C in the Ar atmosphere for 3 h, Ru–Cr_2O_3/NG was obtained.

2.2 Electrochemical measurements

Electrochemical measurements were performed in an alkaline (1 M KOH) and neutral (PBS solution, pH = 7) media, respectively. The electrochemical cell was equipped with the conventional three-electrode cell involving a commercial glass carbon electrode (GCE) with a diameter of 5 mm, a graphite rod electrode, and a saturated calomel electrode (SCE), which served as the working electrode, counter electrode, and reference electrode, respectively. The working electrodes were fabricated by the following procedure: the ink (catalyst in water, 4 mg mL^{-1}, 15 μL) of the as-prepared materials were dropwise coated onto a glassy carbon disk (mass loading ~0.15 mg Ru cm^{-2}) and dried at room temperature in air. Then 5 μL Nafion solution (0.02 wt%) was cast on the electrode surface to adhere the materials. The current densities were normalized by the geometric surface area of the GCE. The potential *versus* saturated calomel electrode was converted into potential *versus* reversible hydrogen electrode (RHE) according to the following equation: $E_{vs.\ RHE} = E_{vs.\ SCE} + E_{SCE}^{\theta} + 0.059\ pH$.[4]

2.3 Materials characterization

The powder X-ray diffraction (XRD) analysis was carried out on a Rigaku D/max 2500PC diffractometer. The morphologies of the samples were observed by a Supra55 field-emission scanning electron microscope (Zeiss, Germany) and a JEM 2100 transmission electron microscope (JEOL, Japan), respectively. Component analysis of the materials was accomplished by X-ray photoelectron spectroscopy (XPS, ESCALAB 250Xi, Thermo Fisher Scientific, USA). The electrochemical measurements were carried out on a CHI 660D electrochemical workstation.

2.4 Theoretical calculations

First-principles calculations were carried out using the Vienna *Ab initio* Simulation Package (VASP).[29] Generalized gradient approximation parameterized by Perdew–Burke–Ernzerholf[30] with spin-polarization was adopted to describe Ru surface slab. Plane-wave subset with an energy cut off of 520 eV and $4 \times 4 \times 1$ *Γ*-centered *k*-points was used. The surface slab of Ru has 16 atoms per layer, with 4 atomic layers in full atomic position relaxation. Hydrogen adsorption sites have been tried on multiple high-symmetry surface positions, ending up with stable minimal points. Detailed Ru, Cr_2O_3 and NG slab structures are shown in Fig. S1.†

3. Results and discussion

3.1 The fabrication and characterization of Ru–Cr_2O_3/NG

The fabrication of Ru–Cr_2O_3/NG was performed by the pyrolysis of $Ru(bpy)_3$ and $Cr(NO_3)_3$ with NG, as shown in Fig. 1a. The Ru precursors including $Ru(bpy)_3$, ruthenium chloride and ruthenium acetylacetonate were screened, and found that $Ru(bpy)_3$ is more suitable to obtain the homogenous Ru nanoparticle. NG used here is our previously reported three-dimensional (3D) porous graphene with high surface area, robust structure and abundant doped nitrogen.[28] NG plays the role of the support as well as the catalyst to boost hydrogen evolution. The composite material was first characterized by X-ray diffraction (XRD), shown in Fig. 1b. The XRD pattern shows a very wide peak centred at 26°, which is attributed to the C (002) diffraction peak of NG. Besides, it also displays a set of sharp and intense peaks located at 38.4°, 42.2°, 44.0°, 58.3°, 69.4°, 78.4°, 82.2°, 84.7°, and 86.0°, which are assigned to the diffraction peaks of hcp-Ru (100), (002), (101), (102), (110), (103), (200), (112) and (201), respectively. The strong diffraction peaks demonstrate that the as-obtained hcp-Ru holds good crystallinity. As we reported previously, the high crystallinity of hcp-Ru is helpful for HER.[31] Additionally, the XRD pattern exhibits a set of very weak peaks positioned at 33.6°, 36.2°, and 54.8°, which are ascribed to the diffraction of Cr_2O_3 (012), (110), and (116), respectively. The intensity of these peaks increases with the number of Cr_2O_3 (Fig. S2†). In comparison with those in the standard card, the position of Ru and Cr_2O_3 fails to exhibit any shifts, indicating that Ru and Cr_2O_3 do not form a new phase, but simply mix together.

The morphologies of Ru–Cr_2O_3/NG were then observed by scanning electron microscopy (SEM) and transmission electron microscopy (TEM), which is shown in Fig. S3† and 2a. The SEM image reveals that the material bears the 3D porous structure. TEM images clearly show the ultrafine Ru and Cr_2O_3

© 2021 The Author(s). Published by the Royal Society of Chemistry

Open Access Article. Published on 03 February 2021. Downloaded on 2/8/2026 6:22:50 PM.
This article is licensed under a Creative Commons Attribution-NonCommercial 3.0 Unported Licence.

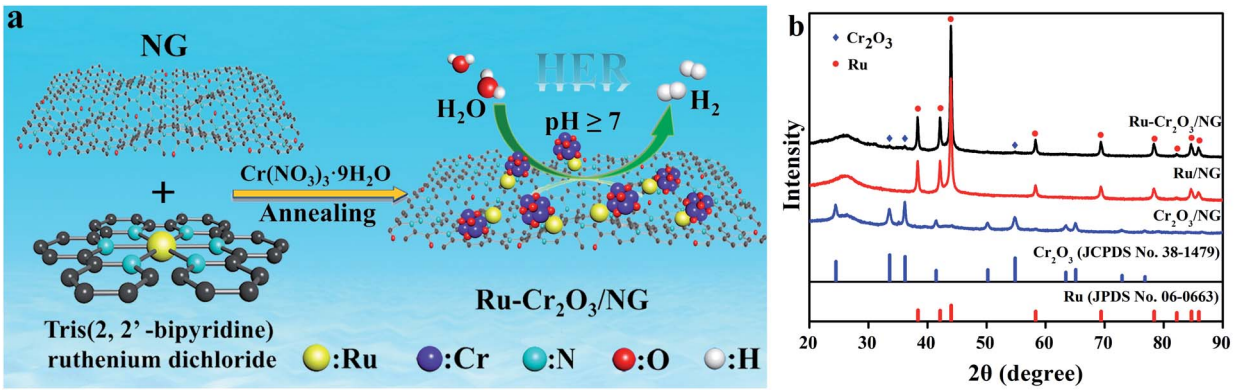

Fig. 1 Schematic illustration of the fabrication of Ru–Cr_2O_3/NG (a), XRD pattern of Ru–Cr_2O_3/NG, Ru/NG and Cr_2O_3/NG(b).

nanoparticles, which are homogeneously decorated on the surface of NG (Fig. 2a). The particles feature a diameter of 2–5 nm. High-resolution TEM (HRTEM) displays the clear crystal lattice fringes, suggesting their good crystallinity (Fig. 2b). The lattice spacing of 0.210 nm and 0.236 nm are assigned to (100) and (101) of hcp-Ru (Fig. 2b),[32] and those of 0.248 nm and 0.363 nm are indexed to (110) and (012) of Cr_2O_3.[33] The results agree well with those of XRD (Fig. 1b) and fast-Fourier transition (FFT) pattern (inset in Fig. 2b). High-angle annular dark-field (HAADF) images by scanning transmission electronic microscopy (STEM) signify the well-dispersed Cr_2O_3 and Ru nanocrystals on NG as well (Fig. 2c). The corresponding elemental mapping analysis unravels the homogeneously distributed elements of C, N, O, Cr, and Ru.

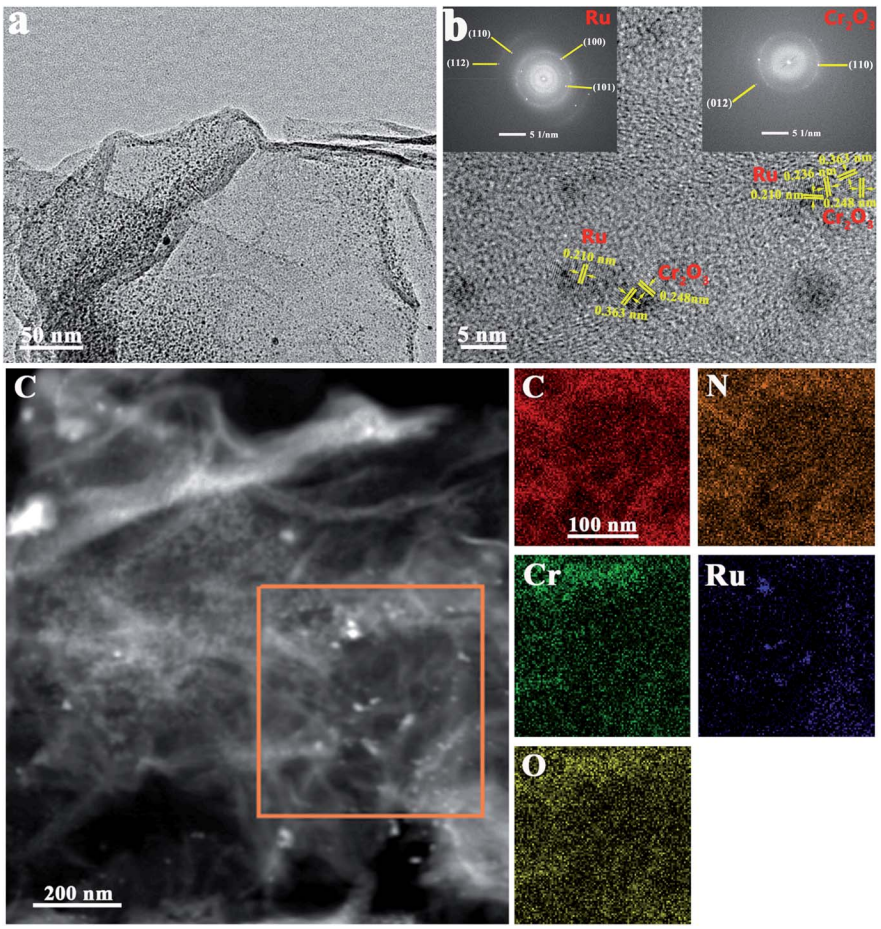

Fig. 2 TEM (a), HRTEM (b), STEM (c) images of Ru–Cr_2O_3/NG, and the corresponding elemental mapping of C, N, Cr, Ru and O. The insets in (b) are the FFT images of Ru and Cr_2O_3.

Open Access Article. Published on 03 February 2021. Downloaded on 2/8/2026 6:22:50 PM. This article is licensed under a Creative Commons Attribution-NonCommercial 3.0 Unported Licence.

The structure of Ru–Cr_2O_3/NG was further analysed by X-ray photoelectron spectroscopy (XPS), as shown in Fig. 3. XPS survey demonstrates the presence of C, N, O, Cr, and Ru as well (Fig. S4†). The atomic contents of Ru, Cr, and N in the composite are 8.62%, 1.72%, and 7.71%, respectively. Ru 3d spectra present peaks centred at 279.5 eV and 284.8 eV (Fig. 3b), indicating the metallic state of Ru.[34] The Cr 2p spectra display peaks positioned at 576.3 eV and 586.5 eV corresponding to Cr $2p_{3/2}$ and Cr $2p_{1/2}$, respectively, evidencing the presence of Cr^{3+} associated with Cr_2O_3.[35] Specially, Cr 2p XPS of Ru–Cr_2O_3/NG exhibited a significant positive shift relative to Cr_2O_3/NG (Fig. 3b), but Ru 3d XPS did not, implying that the addition of Ru led to electron donation from Cr species to NG. The good electroconductivity of Ru possibly boosts the transportation of electrons.[36,37] The peak at 527.8 eV in O 1s XPS is assigned to the surface lattice oxygen (O^{2-}) combined with Cr^{3+}.[38,39] The N 1s XPS verifies the structures of graphitic N, pyrrolic N, and pyridinic N, which are identical to our previously reported NG (Fig. 3d).[26]

3.2 The electrocatalytic performance of Ru–Cr_2O_3/NG in alkaline media

The electrocatalytic performance of our designed Ru–Cr_2O_3/NG for HER was firstly assessed in 1.0 M KOH solution in a three-electrode system using SCE as the reference electrode, graphite rod as the counter electrode, and Ru–Cr_2O_3/NG coated GCE as the working electrode. For the convenience of comparison, the potential *vs.* SCE was converted to that against RHE. As a control experiment, the HER performance of Ru/C, Ru/NG, and Cr_2O_3/NG was also tested, and compared with those of the commercial Pt/C (20 wt%) catalyst. The mass contents of Ru (~17 wt%) and Cr (~1.8 wt%) in each catalyst are maintained at the same level as determined by the inductive coupled plasma-atomic emission spectrometry (ICP-AES) method (Table S1†). The molar ratio of Ru to Cr_2O_3 in Ru–Cr_2O_3/NG was explored before comparison (Fig. S5†). An increase in the amount of Ru will decrease the content of Cr_2O_3. We found that the optimal molar ratio of Ru to Cr_2O_3 is 5 : 1. The catalysts have the identical Ru loading on GCE. Their LSV curves were collected in Fig. 4a. It can be seen that the overpotential needed to achieve the current density of 10 mA cm^{-2} (η_{10}) by the Ru–Cr_2O_3/NG is only 47 mV, which is lower than that of Pt/C catalyst (56 mV), Ru/NG (76 mV) and Ru/C (80 mV). Cr_2O_3/NG hardly exhibits HER activity in alkaline condition. The Tafel plots evidence that Ru–Cr_2O_3/NG presents a slope of 39 mV dec^{-1}, lower than those of Ru/C (62 mV dec^{-1}), Ru/NG (56 mV dec^{-1}), and Pt/C (46 mV dec^{-1}) (Fig. 4b). In alkaline condition, the electrochemical active surface area (ECSA) of a catalyst is generally evaluated by a double layer capacitance (C_{dl}) measurement.[40] As seen in Fig. S6,† Ru–Cr_2O_3/NG exhibits the highest C_{dl} of 25 mF cm^{-2}. Turnover frequency (TOF) is the best figure-of-merit to comparatively evaluate the catalytic activity of different

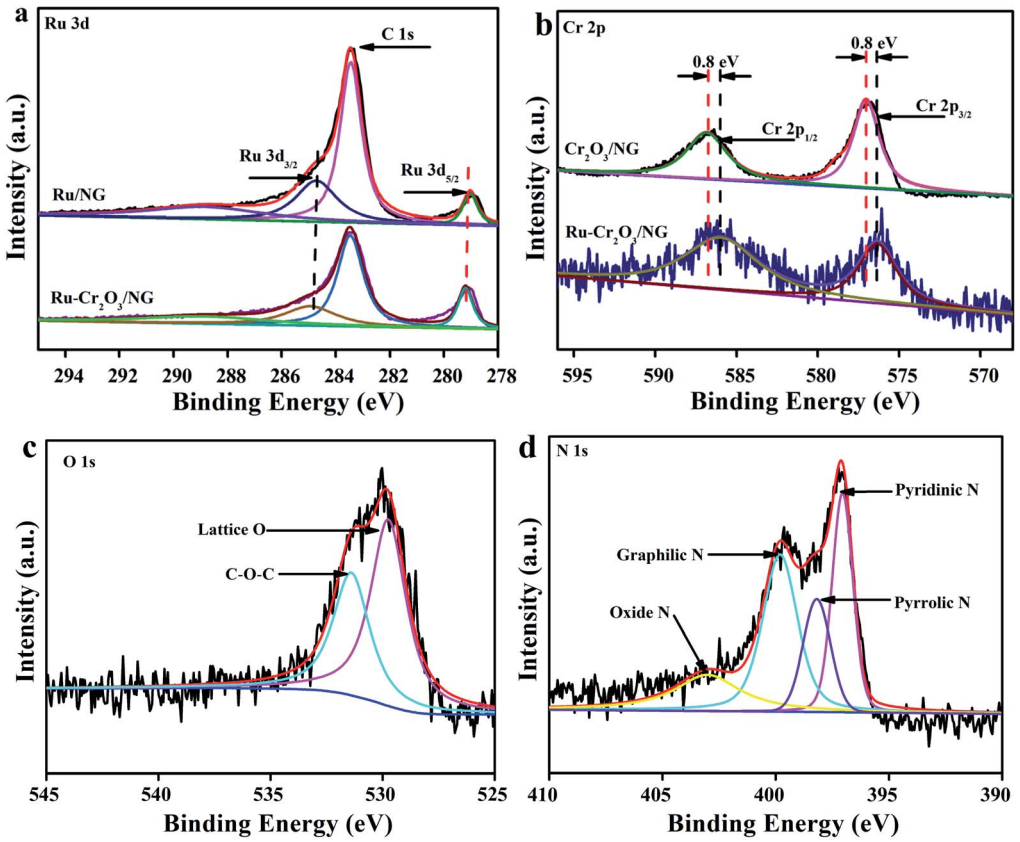

Fig. 3 Ru 3d (a), Cr 2p (b), O 1s (c) and N 1s (d) XPS of Ru–Cr_2O_3/NG.

© 2021 The Author(s). Published by the Royal Society of Chemistry

Open Access Article. Published on 03 February 2021. Downloaded on 2/8/2026 6:22:50 PM.
This article is licensed under a Creative Commons Attribution-NonCommercial 3.0 Unported Licence.

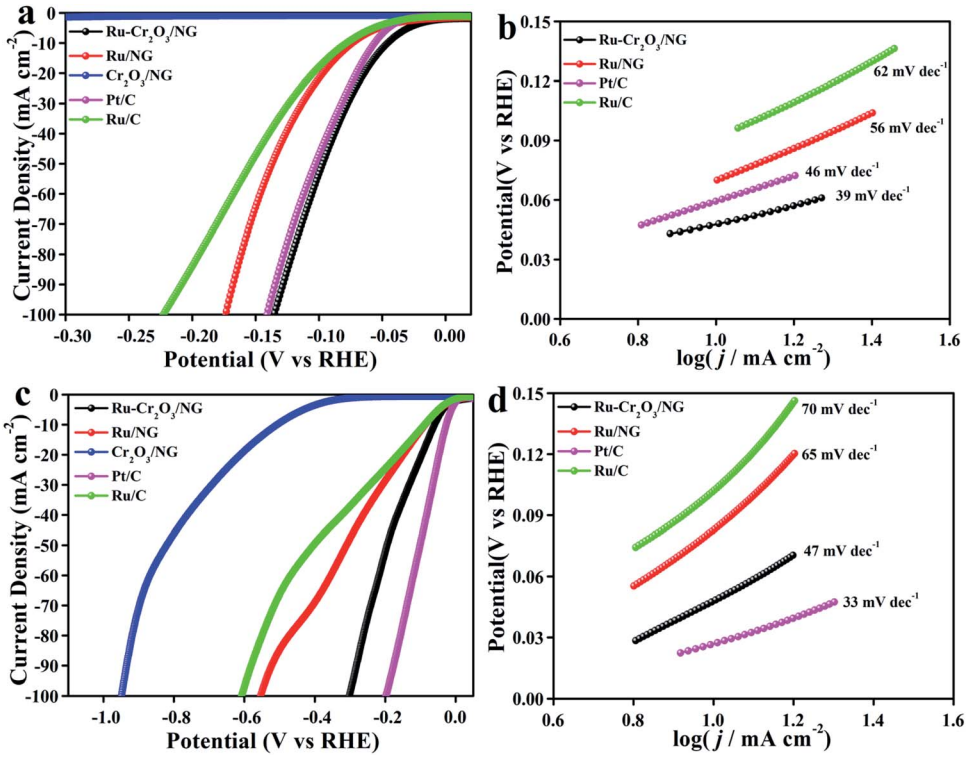

Fig. 4 Electrocatalytic HER activity of catalysts in alkaline (a and b) and neutral (c and d) medium. LSV curves (a and c), Tafel plots (b and d), Catalyst loading: 0.15 mg Ru cm^{-2} on GCE, scan rate: 1 mV s^{-1}.

catalysts. The TOF value of Ru–Cr_2O_3/NG (6.4 s^{-1}) at 100 mV is three times more than that of Ru/NG (2.1 s^{-1}) and five times more than that of Ru/C (1.2 s^{-1}) (Fig. S7†). Electrochemical impedance spectra (EIS) suggest the lowest charge-transfer resistance of Ru–Cr_2O_3/NG (Fig. S8†). Additionally, LSV plots after 20 000 CV cycles and *i–t* curves reveal that Ru–Cr_2O_3/NG bears excellent long-term stability (Fig. S9†). The TEM image shows that after a long-term test, the particles still maintain the highly dispersed state (Fig. S10†). As a result, Ru–Cr_2O_3/NG is an intriguing HER catalyst in alkaline condition, which even possesses excellent activity outperforming most of the previously reported Ru-based catalysts (Table S2†) and the state-of-the-art Pt/C catalyst. Particularly, the existence of Cr_2O_3 and NG can both favour the HER activity of Ru in an alkaline environment.

3.3 The electrocatalytic performance of Ru–Cr_2O_3/NG in neutral media

The electrocatalytic performance of the catalysts was further tested in a neutral media (1 M PBS, pH = 7). As shown in Fig. 4c and d, Ru–Cr_2O_3/NG gives a η_{10} of 53 mV, which is much lower than that of Ru/NG (86 mV), and Ru/C (89 mV). Meanwhile, Ru–Cr_2O_3/NG bears the Tafel slope of 47 mV dec^{-1}, lower than that of Ru/NG (65 mV dec^{-1}) and Ru/C (70 mV dec^{-1}). The mechanism of the enhanced HER activity of Ru by Cr_2O_3 and NG was finally explored. As reported, the pathway of HER in alkaline and neutral media involves the first step of breaking the H–O bond in H_2O to form an adsorbed H* (Volmer reaction) and the second step of combining the adsorbed H* with another H from water dissociation (Heyrovsky reaction) or with another adsorbed H* on a neighbouring active site (Tafel reaction). Therefore, HER is theoretically performed by Volmer–Heyrovsky or Volmer–Tafel route, which can be estimated by the Tafel slope.[41]

These results verified that the HER activity of Ru is also significantly promoted by the introduction of NG and Cr_2O_3 in the neutral condition. Additionally, Ru–Cr_2O_3/NG also exhibits negligible performance loss after a long-term test (Fig. S11†), hinting its practical application potential.

3.4 Theoretical calculation

The mechanism of the enhanced HER activity of Ru by Cr_2O_3 and NG was finally explored. As reported, the pathway of HER in alkaline and neutral media involves the first step of breaking the H–O bond in H_2O to form an adsorbed H* (Volmer reaction) and the second step of combining the adsorbed H* with another H from water dissociation (Heyrovsky reaction) or with another adsorbed H* on a neighbouring active site (Tafel reaction). Therefore, HER is theoretically performed by Volmer–Heyrovsky or Volmer–Tafel route, which can be estimated by the Tafel slope.[41] As seen from Fig. 4b and d, the Tafel slope signifies that these catalysts adopt the Volmer–Heyrovsky pathway, in which the sluggish dissociation of H_2O is the rate-determining step of the HER. The results are consistent with those reported in the literature,[42] and a similar Volmer–Heyrovsky pathway for hcp-Ru/NG was observed. To clarify the effect of NG and Cr_2O_3, density functional theory (DFT) was used to

Open Access Article. Published on 03 February 2021. Downloaded on 2/8/2026 6:22:50 PM.
This article is licensed under a Creative Commons Attribution-NonCommercial 3.0 Unported Licence.

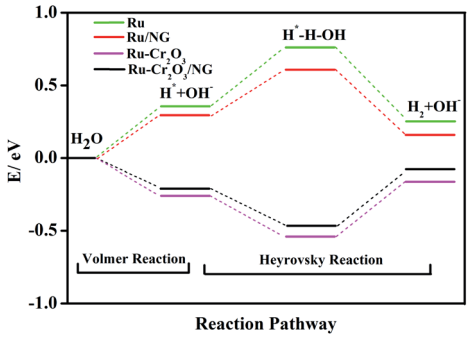

Fig. 5 Energy diagram of the HER in alkaline condition on different surfaces.

calculate the HER activation energy on the surface of Ru, Ru/NG, Ru–Cr_2O_3, and Ru–Cr_2O_3/NG, as shown in Fig. 5. It can be clearly found that, in the first Volmer reaction, the energy barriers to form the first H* decrease from 0.35 eV of Ru to 0.29 eV, 0.27 eV, 0.21 eV of Ru-NG, Ru–Cr_2O_3 and Ru–Cr_2O_3/NG, respectively. Similarly, in the second Heyrovsky reaction, the energy barriers to form the second H decrease from 0.5 eV of Ru to 0.45 eV, 0.36 eV and 0.4 eV, respectively. As a result, the Gibbs free energy of hydrogen evolution on the Ru surface decreases to only 0.08 eV. The intrinsic reason of the decrease of the Gibbs free energy is mainly attributed to the enhanced water-dissociation capability by Cr_2O_3 and NG (Table S3†). Additionally, the electron transportation between Ru, Cr_2O_3, and NG may facilitate the HER activity as well.

4. Conclusions

In summary, we designed a catalyst based on Ru, Cr_2O_3, and NG for HER. The catalyst can function well in alkaline and neutral media. Especially in alkaline condition, Ru–Cr_2O_3/NG shows an outstanding HER performance outperforming Pt/C. In combination with the DFT calculation, the significantly enhanced HER activity of Ru is found to be attributed to the promoted water-dissociation capability by NG and Cr_2O_3, which can bind strongly with H and OH, respectively. The strategy proposed here, multi-site acceleration of water dissociation, is confirmed as an effective way to boost HER activity, which provides new guidance on the design of highly efficient, inexpensive, and biocompatible HER catalysts in nonacidic media.

Conflicts of interest

There are no conflicts to declare.

Acknowledgements

This work is financially supported by the project of Jiangsu Key Laboratory of Advanced Catalytic Materials and Technology, and the Advanced Catalysis and Green Manufacturing Collaborative Innovation Centre of Jiangsu Province.

Notes and references

1 I. Staffell, D. Scamman, A. V. Abad, P. Balcombe, P. E. Doods, P. Ekins, N. Shah and K. R. Ward, *Energy Environ. Sci.*, 2019, **12**, 463.
2 C. Wei, R. R. Rao, J. Y. Peng, B. T. Huang, I. E. L. Stephens, M. Risch, Z. C. J. Xu and Y. Shao-Horn, *Adv. Mater.*, 2019, **31**, 1806296.
3 J. Q. Tian, Q. Liu, A. M. Asiri and X. P. Sun, *J. Am. Chem. Soc.*, 2014, **136**, 7587.
4 H. Y. Jin, J. Wang, D. F. Su, Z. Z. Wei, Z. F. Pang and Y. Wang, *J. Am. Chem. Soc.*, 2015, **137**, 2688.
5 M. K. Kundu, R. Mishra, T. Bhowmika and S. Barman, *J. Mater. Chem. A*, 2018, **6**, 23531.
6 Q. Zhang, W. J. Han, Z. X. Xu, Y. L. Li, L. Chen, Z. Y. Bai, L. Yang and X. L. Wang, *RSC Adv.*, 2020, **10**, 27788.
7 Y. N. Guo, T. Park, J. W. Yi, J. Henzie, J. Kim, Z. L. Wang, B. Jiang, Y. Bando, Y. Sugahara, J. Tang and Y. Yamauchi, *Adv. Mater.*, 2019, **31**, 1807134.
8 X. R. Ding, T. Yang, W. X. Wei, Y. H. Wang, K. Xu, Z. Z. Zhu, H. Zhao, T. T. Yu and D. E. Zhang, *Catal. Sci. Technol.*, 2020, **10**, 3247.
9 C. Q. Huang, L. Yu, W. Zhang, Q. Xiao, J. Q. Zhou, Y. L. Zhang, P. F. An, J. Zhang and Y. Yu, *Appl. Catal., B*, 2020, **276**, 119137.
10 P. Xiao, W. Chen and X. Wang, *Adv. Energy Mater.*, 2015, **5**, 1500985.
11 H. Wu, H. Huang, J. Zhong, Y. Song, Q. B. Zhang and X. C. Zeng, *Nanoscale*, 2019, **11**, 12210.
12 B. O. Baird, J. P. S. Sousa, Y. Ziouani, D. Y. Petrovykh, N. A. Zarkevich, D. D. Johnson, Y. V. Kolen'ko and K. Kovnir, *Chem. Sci.*, 2020, **11**, 5007.
13 X. Y. Wang, Y. Fei, W. Li, L. Y. Yi, B. M. Feng, Y. X. Pan, W. H. Hu and C. M. Li, *ACS Appl. Mater. Interfaces*, 2020, **12**, 16548.
14 H. Vrubel and X. L. Hu, *Angew. Chem., Int. Ed.*, 2012, **51**, 12703.
15 R. Kumar, Z. Ahmed, H. Kaur, C. Bera and V. Bagchi, *Catal. Sci. Technol.*, 2020, **10**, 2213.
16 L. X. Guo, Y. Y. Liu, X. Teng, Y. L. Niu, S. Q. Gong and P. Z. F. Chen, *ChemSusChem*, 2020, **13**, 3671.
17 W. F. Chen, J. T. Muckerman and E. Fujita, *Chem. Commun.*, 2013, **49**, 8896.
18 B. B. Wei, F. W. Ming, H. F. Liang, Z. B. Qi, W. S. Hu and Z. C. Wang, *J. Power Sources*, 2021, **481**, 228842.
19 Y. W. Hu, T. Z. Xiong, M. S. J. T. Balogun, Y. C. Huang, D. Adekoya, S. Q. Zhang and Y. X. Tong, *Mater. Today*, 2020, **15**, 100267.
20 R. Subbaraman, D. Tripkovic, D. Strmcnik, K. C. Chang, M. Uchimura, A. P. Paulikas, V. Stamenkovic and N. M. Markovic, *Science*, 2011, **334**, 1256.
21 Y. Zheng, Y. Jiao, Y. H. Zhu, L. H. Li, Y. Han, Y. Chen, M. Jaroniec and S. Z. Qiao, *J. Am. Chem. Soc.*, 2016, **138**, 16174.
22 M. Gong, W. Zhou, M. J. Kenney, R. Kapusta, S. Cowley, Y. P. Wu, B. G. Lu, M. C. Lin, D. Y. Wang, J. Yang,

© 2021 The Author(s). Published by the Royal Society of Chemistry

Open Access Article. Published on 03 February 2021. Downloaded on 2/8/2026 6:22:50 PM.
This article is licensed under a Creative Commons Attribution-NonCommercial 3.0 Unported Licence.

B. J. Hwang and H. J. Dai, *Angew. Chem., Int. Ed.*, 2015, **54**, 11989.

23 K. Mudiyanselage, S. D. Senanayake, L. Feria, S. Kundu, A. E. Baber, J. Graciani, A. B. Vidal, S. Agnoli, J. Evans, R. Chang, S. Axnanda, Z. Liu, J. F. Sanz, P. Liu, J. A. Rodriguez and D. J. Stacchiola, *Angew. Chem., Int. Ed.*, 2013, **52**, 5101.

24 C. T. Dinh, A. Jain, F. P. G. Arquer, P. D. Luna, J. Li, N. Wang, X. L. Zheng, J. Cai, B. Z. Gregory, O. Voznyy, B. Zhang, M. Liu, D. Sinton, E. J. Crumlin and E. H. Sargent, *Nat. Energy.*, 2019, **4**, 107.

25 W. J. Mitchell, J. Xie, T. A. Jachimowski and W. H. Weinberg, *J. Am. Chem. Soc.*, 1995, **117**, 2606.

26 Y. T. Li, F. Q. Chu, Y. F. Bu, Y. Kong, Y. X. Tao, X. Zhou, H. R. Yu, J. J. Yu, L. Tang and Y. Qin, *Chem. Commun.*, 2019, **55**, 7828.

27 X. K. Kong, K. Xu, C. L. Zhang, J. Dai, S. N. Oliaee, L. Y. Li, X. C. Zeng, C. Z. Wu and Z. M. Peng, *ACS Catal.*, 2016, **6**, 1487.

28 Y. Qin, J. Yuan, J. Li, D. C. Chen, Y. Kong, F. Q. Chu, Y. X. Tao and M. L. Liu, *Adv. Mater.*, 2015, **27**, 5171.

29 G. Kresse and J. Furthmuller, *Comput. Mater. Sci.*, 1996, **6**, 15.

30 J. P. Perdew, K. Burke and M. Ernzdrhol, *Phys. Rev. Lett.*, 1996, **77**, 3865.

31 Y. T. Li, L. A. Zhang, Y. Qin, F. Q. Chu, Y. Kong, Y. X. Tao, Y. X. Li, Y. F. Bu, D. Ding and M. L. Liu, *ACS Catal.*, 2018, **8**, 5714.

32 Y. T. Li, F. Q. Chu, Y. Liu, Y. Kong, Y. X. Tao, Y. X. Li and Y. Qin, *Chem. Commun.*, 2018, **54**, 13076.

33 Y. Zhao, J. J. Wang, C. L. Ma and Y. Li, *Chem. Phys. Lett.*, 2018, **704**, 31.

34 J. W. Liu, G. Z. Ding, J. Y. Yu, X. G. Liu, X. F. Zhang, J. J. Guo, J. C. Zhang, W. Ren and R. C. Che, *J. Mater. Chem. A*, 2019, **7**, 18072.

35 Y. Zhang, W. B. Qiu, Y. J. Ma, Y. L. Luo, Z. Q. Tian, G. W. Cui, F. Y. Xie, L. Chen, T. S. Li and X. P. Sun, *ACS Catal.*, 2018, **8**, 8540.

36 G. Meng, H. Tian, L. X. Peng, Z. H. Ma, Y. F. Chen, C. Chen, Z. W. Chang, X. Z Cui and J. L. Shi, *Nano Energy*, 2021, **80**, 105531.

37 A. M. Abdel-Mageed, K. Wiese, M. Parlinska-Wojtan, J. Rabeah, A. Brückner and R. J. Behm, *Appl. Catal., B*, 2020, **270**, 118846.

38 F. Yang, W. J. Bao, T. X. Liu, B. Zhang, S. Huang, W. Yang, Y. Li, N. Li, C. X. Wang, C. W. Pan and Y. F. Li, *Microchim. Acta*, 2020, **187**, 322.

39 S. X. Yang, W. P. Zhu, Z. P. Jiang, Z. X. Chen and J. B. Wang, *Appl. Surf. Sci.*, 2006, **252**, 8499.

40 J. J. Bai, Q. Q. Sun, Z. L. Wang and C. Zhao, *J. Electrochem. Soc.*, 2017, **164**, H587.

41 S. H. Ye, F. Y. Luo, T. T. Xu, P. Y. Zhang, H. D. Shi, S. Q. Qin, J. P. Wu, C. X. Wu, X. P. Ouyang, Q. L. Zhang, J. H. Liu and X. L. Sun, *Nano Energy*, 2020, **68**, 104301.

42 Z. L. Wang, X. F. Hao, Z. Jiang, X. P. Sun, D. Xu, J. Wang, H. X. Zhong, F. L. Meng and X. B. Zhang, *J. Am. Chem. Soc.*, 2015, **137**, 15070.

© 2021 The Author(s). Published by the Royal Society of Chemistry